

Alignment of quasar polarizations with large-scale structures[★]

D. Hutsemékers¹, L. Braibant¹, V. Pelgrims¹, D. Sluse²

¹ Institut d’Astrophysique et de Géophysique, Université de Liège, Allée du 6 Août 17, B5c, B-4000 Liège, Belgium

² Argelander-Institut für Astronomie, Auf dem Hügel 71, 53121 Bonn, Germany

Received ; accepted:

ABSTRACT

We have measured the optical linear polarization of quasars belonging to Gpc-scale quasar groups at redshift $z \sim 1.3$. Out of 93 quasars observed, 19 are significantly polarized. We found that quasar polarization vectors are either parallel or perpendicular to the directions of the large-scale structures to which they belong. Statistical tests indicate that the probability that this effect can be attributed to randomly oriented polarization vectors is of the order of 1%. We also found that quasars with polarization perpendicular to the host structure preferentially have large emission line widths while objects with polarization parallel to the host structure preferentially have small emission line widths. Considering that quasar polarization is usually either parallel or perpendicular to the accretion disk axis depending on the inclination with respect to the line of sight, and that broader emission lines originate from quasars seen at higher inclinations, we conclude that quasar spin axes are likely parallel to their host large-scale structures.

Key words. Quasars: general – Polarization – Large-scale structure of Universe

1. Introduction

Hutsemékers et al. (1998, 2001, 2005, hereafter Papers I, II, III) have reported alignments of quasar optical linear polarizations extending over Gpc-scale regions of the sky at redshift $z \sim 1$ (see also Jain et al. 2004, Shurtleff 2013, Pelgrims and Cudell 2014). Possible effects modifying the polarization of light along the line of sight, in particular mixing with axion-like particles, have been investigated in details (e.g., Das et al. 2005, Agarwal et al. 2012). However, due to the absence of comparable circular polarization, these mechanisms have been essentially ruled out (Hutsemékers et al. 2010, Payez et al. 2011).

Since quasar polarization is often related to the object geometry, another interpretation would be that quasars themselves are aligned, presumably with the structure to which they belong. To test this hypothesis, we have measured the polarization of quasars belonging to the large quasar group (LQG) constituted of the groups U1.27 (aka Huge-LQG) and U1.28 (aka CCLQG) described in Clowes et al. (2013). These quasar structures extend over Gpc scales at redshift $z \sim 1.3$, possibly beyond the homogeneity scale of the concordance cosmology (~ 370 Mpc, Yadav et al. 2010; but see Nadathur 2013, Einasto et al. 2014).

2. Observations and polarization measurements

Observations were carried out at the European Southern Observatory, Paranal, on March 22-26, 2014, using the Very Large Telescope equipped with the FORS2 instrument in the standard imaging polarimetry mode IPOL¹. Linear polarimetry is performed by inserting in the parallel beam a Wollaston prism which splits the incoming light rays into two orthogonally polarized beams separated by $22''$. Image overlapping is avoided by inserting a special mask in the focal plane. To measure the

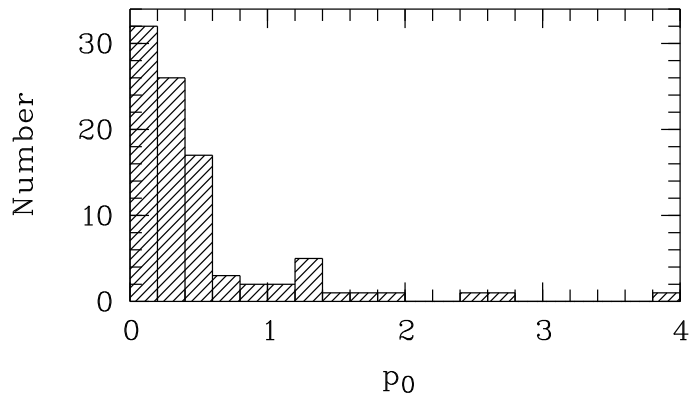


Fig. 1. The distribution of the debiased polarization degree p_0 (in %) measured for the sample of 93 quasars.

normalized Stokes parameters q and u , 4 frames are obtained with the half-wave plate rotated at 4 position angles, 0° , 22.5° , 45° , and 67.5° . This procedure allows us to remove most of the instrumental polarization. The linear polarization degree p and position angle θ are derived using $p = (q^2 + u^2)^{1/2}$ and $\theta = 1/2 \arctan(u/q)$ so that $q = p \cos 2\theta$ and $u = p \sin 2\theta$. Since orthogonally polarized images of the object are simultaneously recorded, the measured polarization does not depend on variable transparency or seeing.

All observations were obtained using the FORS2 V_high filter ($\lambda_0 = 555$ nm, FWHM = 123 nm). Data reduction and measurements were performed as detailed in Sluse et al. (2005). The instrumental polarization was checked using the unpolarized stars WD0752–676 and WD1615–154 (Fossati et al. 2007) and found to be $p = 0.05 \pm 0.06\%$, which is consistent with zero². Note that we did not use field stars to estimate

[★] Based on observations made with ESO Telescopes at the La Silla Paranal Observatory under programme ID 092.A-0221

¹ FORS User Manual, VLT-MAN-ESO-13100-1543, Issue 92.0

² We also observed HD 64299 which turned out to be polarized with $p = 0.17 \pm 0.04\%$, in agreement with Masiero et al. (2007).

Table 2. The sample of 19 quasars with $p \geq 0.6\%$

Object	z	LQG	p (%)	σ_p (%)	θ ($^\circ$)	σ_θ ($^\circ$)	FWHM km s^{-1}	σ_{FWHM} km s^{-1}
SDSSJ105421.90+212131.2	1.2573	1	1.04	0.08	92.6	2.2	5094	214
SDSSJ105446.73+195710.5	1.2195	1	1.89	0.23	75.2	3.5	3256	363
SDSSJ105611.27+170827.5	1.3316	1	1.29	0.08	44.8	1.8	6088	158
SDSSJ110016.88+193624.7	1.2399	1	1.14	0.23	160.4	5.9	3909	348
SDSSJ104445.03+151901.6	1.2336	2	1.25	0.11	167.5	2.5	3254	196
SDSSJ104616.31+164512.6	1.2815	2	1.25	0.11	86.9	2.5	2635	222
SDSSJ104859.74+125322.3	1.3597	2	0.72	0.13	45.6	5.3	3746	397
SDSSJ104941.67+151824.6	1.3390	2	1.31	0.13	146.4	2.9	4034	633
SDSSJ105245.80+134057.4	1.3544	2	1.32	0.11	30.2	2.4	5885	174
SDSSJ105442.71+104320.6	1.3348	2	0.73	0.11	172.8	4.4	4108	269
SDSSJ105525.68+113703.0	1.2893	2	2.55	0.10	49.1	1.1	4443	399
SDSSJ111009.58+075206.8	1.2123	3	1.81	0.17	34.2	2.7	5032	626
SDSSJ111802.11+103302.4	1.2151	3	3.97	0.10	142.4	0.7	6900	1256
SDSSJ104116.79+035511.4	1.2444	4	1.55	0.11	99.7	2.0	2195	296
SDSSJ104225.63+035539.1	1.2293	4	0.69	0.08	23.2	3.3	5182	380
SDSSJ105010.05+043249.1	1.2158	4	2.67	0.08	101.5	0.9	2703	190
SDSSJ105512.23+061243.9	1.3018	4	0.98	0.12	115.9	3.5	3381	299
SDSSJ105833.86+055440.2	1.3222	4	0.62	0.21	37.8	10.3	5167	410
SDSSJ110108.00+043849.6	1.2516	4	0.84	0.10	25.7	3.4	4823	269

Notes. Column 1 gives the quasar SDSS name, column 2 the redshift z , column 3 the quasar group (Fig. 4), columns 4 and 5 the polarization degree p and its error σ_p , columns 6 and 7 the polarization position angle θ and its error σ_θ , columns 8 and 9 the MgII emission line FWHM and its error from Shen et al. (2011).

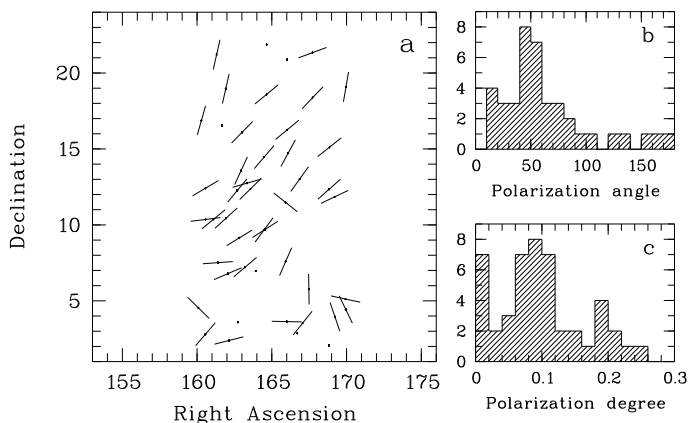


Fig. 2. The interstellar polarization in the region of the sky corresponding to the quasar large-scale structure under study (data from Berdyugin et al. 2014). (a) Map of polarization vectors; right ascensions and declinations are in degree; the length of the polarization vectors is arbitrary. (b) Distribution of polarization angles (in degree). (c) Distribution of polarization degrees (in %).

the instrumental polarization because of spurious off-axis polarization in FORS1/2 (Patat and Romaniello 2006). To fix the zero-point of the polarization position angle, polarized standard stars have been observed: NGC 2024-1, Ve 6-23, CD-28 $^\circ$ 13479, HD 316232, BD-14 $^\circ$ 922 (Fossati et al. 2007). The offset –to subtract from the raw polarization angle– was determined to be $2.5^\circ \pm 0.5^\circ$ in the V_high filter.

The linear polarization of all 73 quasars of the Huge-LQG and of 20 out of the 34 quasars of the CCLQG has been obtained, i.e., for a total of 93 quasars. Table 1 summarizes the measurements. The error on the polarization degree is between 0.06% and 0.23%, with a mean value of 0.12%. The distribution of the debiased polarization degree is illustrated in Fig. 1.

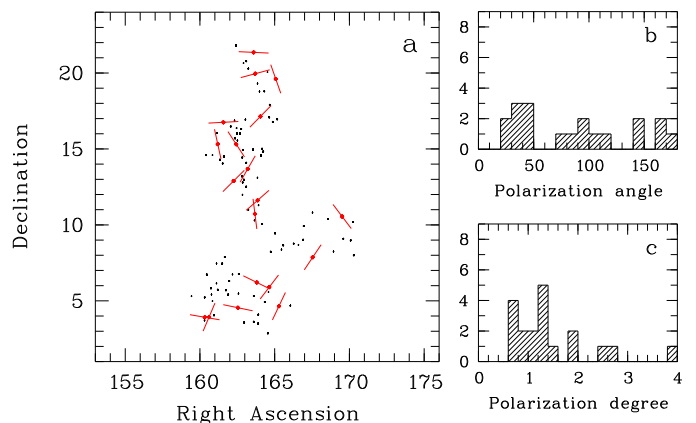


Fig. 3. The polarization of the 19 quasars with $p \geq 0.6\%$. (a) Map of polarization vectors over the large-scale structure; right ascensions and declinations are in degree; the length of the polarization vectors is arbitrary. (b) Distribution of polarization angles (in degree). (c) Distribution of polarization degrees (in %).

It shows a peak near the null value, in agreement with other polarization measurements of radio-quiet non-BAL quasars (Berriman et al. 1990, Hutsemékers et al. 1998b). All objects are at galactic latitudes higher than 50° which minimizes contamination by interstellar polarization. In this region of the sky, the interstellar polarization is around $p_{\text{is}} \approx 0.1\%$ with a peak near 50° (Fig. 2). As in Papers I-III, we consider that polarization is essentially intrinsic to the quasar when $p \geq 0.6\%$ (Berriman et al. 1990, Hutsemékers et al. 1998b, Sluse et al. 2005). Out of 93 quasars, 19 have $p \geq 0.6\%$. Their properties are given in Table 2. For these 19 polarized quasars, $\sigma_\theta \leq 10^\circ$ with an average value around 3° .

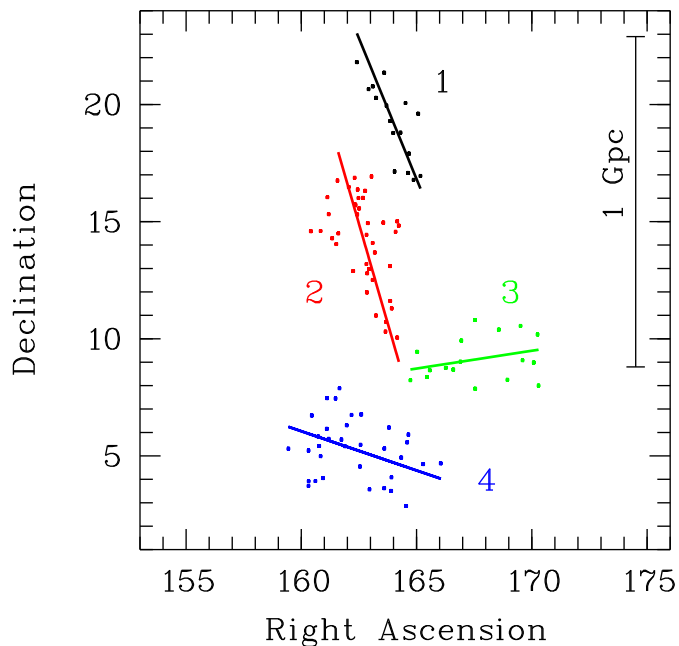


Fig. 4. The quasar groups and their orientations on the sky. Right ascensions and declinations are in degree. The superimposed lines illustrate the orientations of the four groups labelled 1, 2, 3, 4. The comoving distance scale at redshift $z = 1.3$ is indicated assuming a flat Universe with $H_0 = 70 \text{ km s}^{-1} \text{ Mpc}^{-1}$ and $\Omega_m = 0.27$.

3. Analysis of polarization alignments

In Fig. 3 we show a map of the quasar polarization vectors over the LQG structure. The map does not show any evidence for coherent orientations or alignments. The distribution of the polarization angles is flat, compatible with random orientations and with no contamination by interstellar polarization.

In order to compare the quasar polarization angles to the direction of the local structures, we consider four structures for which we determine a mean orientation, as illustrated in Fig. 4. Group 4 is the CCLQG defined in Clowes et al. (2012). The Huge-LQG is divided in groups denoted 1, 2 and 3. Group 3 corresponds to the “branch” set of 17 quasars identified by Clowes et al. (2013). The large vertical part of the Huge-LQG is then separated into groups 1 and 2. The mean projected direction of the structures is determined by an orthogonal regression in right ascension, declination (Isobe et al. 1990). For groups 1, 2, 3, 4, we measure the position angles $PA = 157^\circ, 164^\circ, 81^\circ$, and 109° , respectively. We estimate the acute angle between the quasar polarization vectors and the PA of the structures to which they belong using $\Delta\theta = \min(|PA - \theta|, 180^\circ - |PA - \theta|)$.

The distribution of $\Delta\theta$ is illustrated in Fig. 5. It shows a bimodal distribution, with both alignments ($\Delta\theta \approx 0^\circ$) and anti-alignments ($\Delta\theta \approx 90^\circ$) in each quasar group (except group 3). The cumulative binomial probability to have 9 or more quasars in the first and the last bins is $P_{\text{bin}} = 1.4\%$. The Kuiper test (Arsham 1988, Fisher 1993) gives a probability $P_K = 1.6\%$ that the observed distribution is drawn from an uniform distribution. These results are robust if we consider the 28 quasars with $p \geq 0.5\%$ (in this case $P_{\text{bin}} = 1.2\%$ and $P_K = 1.0\%$).

A bimodal distribution of $\Delta\theta$ is exactly what we expect if the quasar morphological axes are related to the orientation of the host large-scale structures. Indeed, the polarization of type 1 AGN is usually either parallel or perpendicular to the AGN accretion disk axis depending on the inclination with respect to the

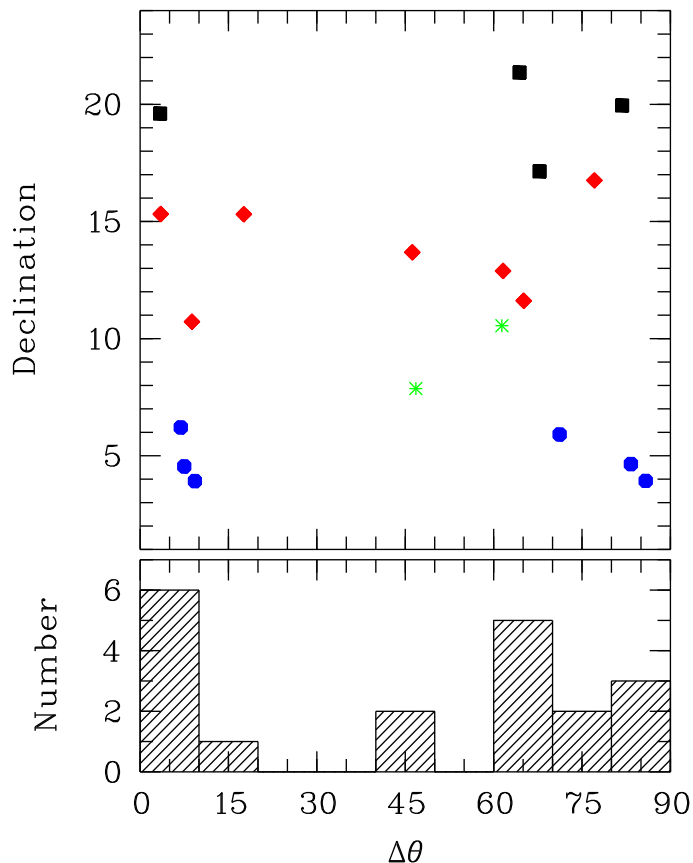


Fig. 5. Bottom: The distribution of the acute angle $\Delta\theta$ (in degree) between quasar polarizations and the orientation of their host large-scale structure. Top: $\Delta\theta$ is plotted against the object declination (in degree) to illustrate the behavior of the different quasar groups (1: squares, 2: lozenges, 3: asterisks, 4: hexagons; colors as in Fig. 4).

line of sight (e.g., Smith et al. 2004). We may assume that higher luminosity AGN (quasars) behave similarly. In Fig. 6, the quasar polarization angles modified according to $\tilde{\theta} = \text{mod}(\theta, 90^\circ) + 90^\circ$ are plotted over the LQG structure, unveiling a remarkable correlation. We stress that such a behavior cannot be due to contamination by interstellar polarization which would align all polarizations similarly.

To quantify the significance of this correlation independently of the shape of the host structure, we use the Andrews and Wasserman Z_c statistical test (Bietenholz 1986, Paper I). This test is best suited to small samples since it does not involve angle dispersion. The idea of the Andrews & Wasserman test is to compute for each object i , the mean direction θ_i of its n_v nearest neighbours, and to compare this local average to the polarization angle of the object i , θ_i . If angles are correlated to positions, one expects, on the average, θ_i to be closer to $\bar{\theta}_{j=i}$ than to $\bar{\theta}_{j \neq i}$. As a measure of the closeness of θ_i and $\bar{\theta}_j$, one uses $D_{i,j} = \mathbf{y}_i \cdot \bar{\mathbf{Y}}_j$, where \mathbf{y}_i is the normalized polarization vector of object i and $\bar{\mathbf{Y}}_j$ the normalized resultant polarization vector of the n_v neighbours of object j , excluding j . Then Z_i is computed by ranking $D_{i,j=i}$ among the $D_{i,j=1,n}$ and the final statistics Z_c is obtained by averaging the Z_i over the sample of n objects. Z_c is expected to be significantly larger than zero when the polarization angles are not randomly distributed over positions. To make the test independent of the coordinate system, polarization vectors can be parallel transported before computing the resultant polarization vectors (Jain et al. 2004). Here, the polarization vectors are com-

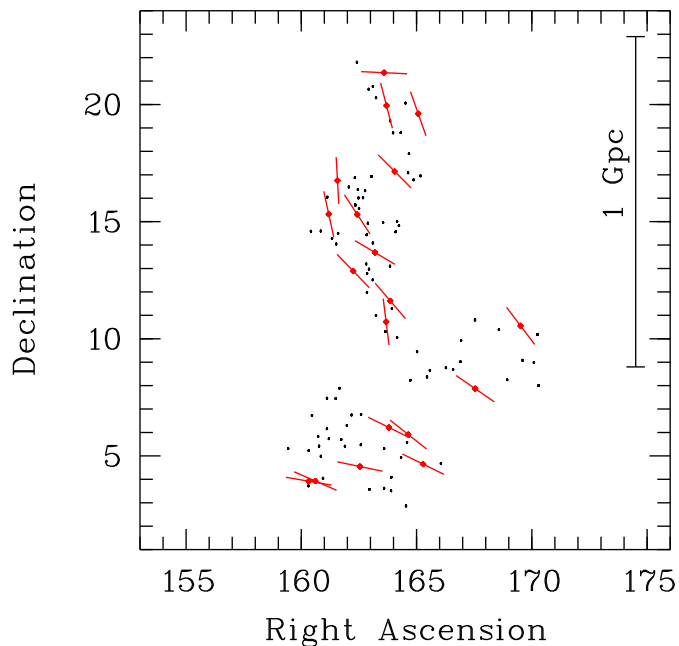


Fig. 6. The polarization vectors of the 19 quasars with $p \geq 0.6\%$ are superimposed on the large-scale structure after rotation of the polarization angles according to $\tilde{\theta} = \text{mod}(\theta, 90^\circ) + 90^\circ$. A clear correlation is seen but we nevertheless caution against exaggerated visual impression since polarization angles are now in the range $[90^\circ - 180^\circ]$. Right ascensions and declinations are in degree. The comoving distance scale is indicated as in Fig. 4.

puted using $\mathbf{y} = (\cos \Theta, \sin \Theta)$ with $\Theta = 4 \text{ mod}(\theta, 90^\circ)$ instead of $\Theta = 2\theta = 2 \text{ mod}(\theta, 180^\circ)$ to test for either alignments or anti-alignments (i.e., dealing with 4-axial data instead of 2-axial data, Fisher 1993). To estimate the statistical significance, 10^5 samples of 19 angles were created through Monte-Carlo simulations either by shuffling the measured angles over positions, or by randomly generating them in the $[0^\circ, 180^\circ]$ range (Press et al. 1992). The significance level (S.L.) of the test is finally computed as the percentage of simulated configurations for which $Z_c \geq Z_c^*$ where Z_c^* is the measured sample statistics. Since all quasars are in a limited redshift range, we only consider their angular positions on the sphere.

The significance level of the Z_c test is illustrated in Fig. 7. It shows that the probability that the polarization angles are randomly distributed over positions is smaller than 1%. The effect is stronger (S.L. $< 0.1\%$) when the mean orientation is computed with 10 nearest neighbours, i.e., roughly half of the sample. This number corresponds to a mean comoving distance of ~ 550 Mpc, in agreement with the trend seen in Fig. 6. Parallel transport has little effect since all quasars lie close to each other and to the equator. We emphasize that a deviation from uniformity is only detected when using $4 \text{ mod}(\theta, 90^\circ)$ in the Z_c test and not when using $2 \text{ mod}(\theta, 180^\circ)$, which means that purely parallel or perpendicular alignments are not seen (Fig. 3). If we consider the 28 quasars with $p \geq 0.5\%$, a similar curve is obtained with the minimum shifted to $n_v = 20$, which corresponds to a mean comoving distance of ~ 650 Mpc.

Since the width of low-ionization emission lines ($H\beta$, MgII) observed in quasar spectra correlates with the object inclination with respect to the line of sight (Wills and Brown 1986, Brotherton 1996, Jarvis and McLure 2006, Decarli et al. 2008), we plot in Fig. 8 the angle $\Delta\theta$ as a function of the quasar MgII emission line width (FWHM from Shen et al. 2011). We see that

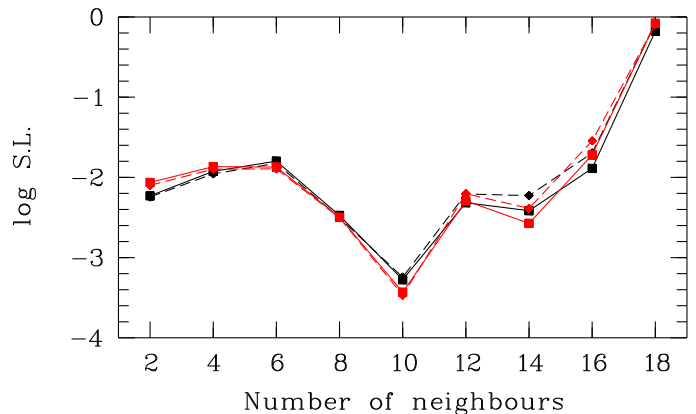


Fig. 7. The logarithm of the significance level (S.L.) of the Z_c test applied to the sample of 19 polarized quasars, as a function of the number of nearest neighbours. The solid line refers to simulations obtained by shuffling angles over positions while the dashed line refers to simulations obtained by randomly generating angles. The statistics are computed with (in red) and without (in black) parallel transport of the polarization vectors.

most objects with polarization perpendicular to the host structure ($\Delta\theta > 45^\circ$) have large emission line widths while all objects with polarization parallel to the host structure ($\Delta\theta < 45^\circ$) have small emission line widths. A two-sample Kolmogorov-Smirnov test indicates that there is a probability of only 1.4% that quasars with either perpendicular or parallel polarizations have emission line widths drawn from the same parent population. Quasars seen at higher inclinations³ generally show broader low-ionization emission lines, in agreement with line formation in a rotating disk (Wills and Brown 1986, Jarvis and McLure 2006, Decarli et al. 2008). The relation seen in Fig. 8 thus supports our hypothesis that the polarization of quasars is either parallel or perpendicular to the host structure depending on their inclination. When rotating by 90° the polarization angles of objects with MgII emission line widths larger than 4300 km s^{-1} , a stronger alignment is seen (Fig. 9). The Kuiper test gives a probability $P_K = 0.5\%$ that the observed distribution is drawn from an uniform distribution. But this value should be seen with caution since the cut at 4300 km s^{-1} is arbitrary. On the other hand, it should be emphasized that the emission line width does not only depend on inclination but also on the mass of the central black hole if the rotating disk is virialized. Quasars with lower black hole mass will have narrower emission lines whatever their inclination so that some of them may still appear anti-aligned in Fig. 9.

Since objects seen at higher inclinations preferentially show polarization perpendicular to their axes (Smith et al. 2004), we finally infer that quasar spin axes should be predominantly parallel to the orientation of the structures to which they belong.

4. Conclusions

We have measured the polarization of 93 quasars belonging to large-scale quasar groups. 19 quasars out of 93 are significantly polarized with $p \geq 0.6\%$.

We found that quasar polarization vectors are either parallel or perpendicular to the large-scale structures to which they belong, and correlated to the polarization vectors of their neighbours. The probability that these results can be attributed to a random distribution of polarization angles is of the order of 1%.

³ Face-on: $i = 0^\circ$. Edge-on: $i = 90^\circ$

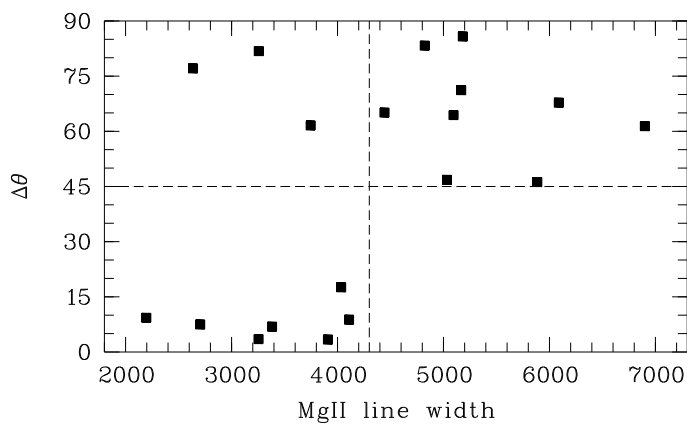


Fig. 8. The angle $\Delta\theta$ (in degree) between quasar polarizations and the orientation of their host large-scale structures as a function of the MgII emission line width (FWHM in km s^{-1}).

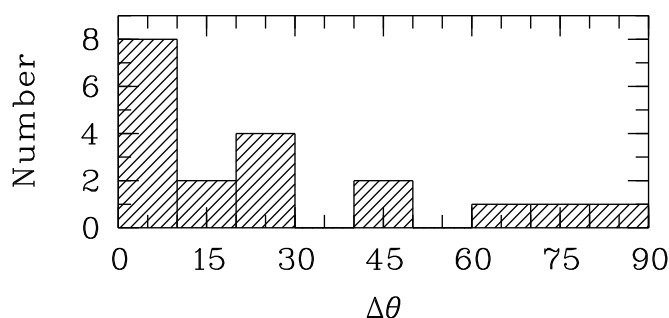


Fig. 9. The distribution of the acute angle $\Delta\theta$ (in degree) between quasar polarizations and the orientation of their host large-scale structure after rotating by 90° the polarization angles of objects with MgII emission line widths larger than 4300 km s^{-1} .

Such a behavior cannot be due to contamination by interstellar polarization. Our results are robust if we consider $p \geq 0.5\%$ instead of $p \geq 0.6\%$, or if we subtract a systematic $p_{\text{is}} = 0.1\%$ at $\theta_{\text{is}} = 50^\circ$ to simulate the correction of a possible contamination by interstellar polarization (Fig. 2).

Assuming that quasar polarization is either parallel or perpendicular to the accretion disk axis as a function of inclination, as observed in lower luminosity AGN, and considering that broader emission lines originate from quasars seen at higher inclinations, we inferred that quasar spin axes are likely parallel to their host large-scale structures.

Galaxy spin axes are known to align with large-scale structures such as cosmic filaments (e.g., Tempel and Libeskind 2013, Zhang et al. 2013, and references therein). Till now, such alignments are detected up to redshift $z \sim 0.6$ at scales $\lesssim 100 \text{ Mpc}$ (Li et al. 2013). Detailed interpretations remain complex because the link between galaxy and halo spin axes is not straightforward, and because the strength and orientation of the alignments depend on several factors, in particular the mass of the halo and the cosmic history (e.g., Hahn et al. 2010, Trowland et al. 2013, Dubois et al. 2014). We have found that quasar accretion disk axes are likely parallel to the large-scale structures to which they belong over Gpc scales at redshift $z \sim 1.3$, i.e., one order of magnitude bigger than currently known galaxy alignments. Although the scales involved are much larger, we may assume that similar mechanisms can explain alignments of quasar and galaxy axes with their host large-scale structure, keeping in mind that polarization-related quasar regions (accretion disk, jet, scattering region) are not necessarily well aligned with the stellar com-

ponent of the host galaxy (Borguet et al. 2008, Hopkins et al. 2012), and that quasars, more prone to strong feedback mechanisms, can have a different cosmic history (Dubois et al. 2014).

Since coherent orientations of quasar polarization vectors, and then quasar axes, are found on scales larger than 500 Mpc , our results might also provide an explanation to the very large-scale polarization alignments reported in Papers I-III. In this case those alignments would be intrinsic and not due to a modification of the polarization along the line of sight. The existence of correlations in quasar axes over such extreme scales would constitute a serious anomaly for the cosmological principle.

Acknowledgements. We thank the referee, E. Tempel, for constructive remarks which helped to improve the paper. We thank B. Borguet, R. Cabanac, J.R. Cudell, H. Lamy and A. Payez for discussions and V. Ivanov for his efficient help during the observations. D.H. and L.B. are respectively Senior Research Associate and Research Assistant at the F.R.S.-FNRS. D.S. acknowledges support from the Deutsche Forschungsgemeinschaft, reference SL172/1-1. This work was supported by the Fonds de la Recherche Scientifique - FNRS under grant 4.4501.05. This research has made use of the NASA/IPAC Extragalactic Database (NED) which is operated by the Jet Propulsion Laboratory, California Institute of Technology, under contract with the National Aeronautics and Space Administration.

References

- Agarwal, N., Aluri, P.K., Jain, P., Khanna, U., Tiwari, P. 2012, EPJC, 72, 1928
 Arsham H. 1988, J. Appl. Stat. 15, 131
 Berdyugin, A., Piirola, V., Teerikorpi, P. 2014, A&A, 561, A24
 Berriman, G., Schmidt, G.D., West, S.C., Stockman, H.S. 1990, ApJS, 74, 869
 Bietenholz, M.F. 1986, AJ, 91, 1249
 Borguet, B., Hutsemékers, D., Letawe, G., Letawe, Y., Magain, P. 2008, A&A, 478, 321
 Brotherton, M.S. 1996, ApJS, 102, 1
 Clowes, R.G., Campusano, L.E., Graham, M.J., Söchting, I.K. 2012, MNRAS, 419, 556
 Clowes, R.G., Harris, K.A., Raghunathan, S., et al. 2013, MNRAS, 429, 2910
 Das, S., Jain, P., Ralston, J.P., Saha, R. 2005, J. Cosmology Astropart. Phys., 06, 002
 Decarli, R., Labita, M., Treves, A., Falomo, R. 2008, MNRAS, 387, 1237
 Dubois, Y., Pichon, C., Welker, C., et al. 2014, MNRAS, 444, 1453
 Einasto, M., Tago, E., Lietzen, H., et al., 2014, A&A, 568, A46
 Fisher, N.I. 1993, Statistical Analysis of Circular Data, Cambridge University Press, Cambridge
 Fossati, L., Bagnulo, S., Mason, E., Landi Degl’Innocenti, E. 2007, ASPC, 364, 503
 Hahn, O., Teyssier, R., Marcella Carollo, C. 2010, MNRAS, 405, 274
 Hopkins, P.F., Hernquist, L., Hayward, C.C. 2012, MNRAS, 425, 1121
 Hutsemékers, D. 1998, A&A, 332, 410 (Paper I)
 Hutsemékers, D., Lamy, H., Remy, M. 1998, A&A, 340, 371
 Hutsemékers, D., Lamy, H. 2001, A&A, 367, 381 (Paper II)
 Hutsemékers, D., Lamy, H., Cabanac, R., Sluse, D. 2005, A&A, 441, 915 (Paper III)
 Hutsemékers, D., Borguet, B., Sluse, D., Cabanac, R., Lamy, H. 2010, A&A, 520, L7
 Isobe, T., Feigelson, E., Akritas, M.G., Babu, G.J. 1990, ApJ, 364, 104
 Jain, P., Narain, G., Sarala, S. 2004, MNRAS, 347, 394
 Jarvis, M.J., McLure, R.J. 2006, MNRAS, 369, 182
 Li, C., Jing, Y.P., Faltenbacher, A., Wang, J. 2013, ApJ, 770, L12
 Masiero, J., Hodapp, K., Harrington, D., Lin, H. 2007, PASP, 119, 1126
 Nadathur, S. 2013, MNRAS, 434, 398
 Patat, F., Romaniello, M. 2006, PASP, 118, 146
 Payez, A., Cudell, J. R., Hutsemékers, D. 2011, Phys. Rev. D, 84, 085029
 Pelgrims, V., Cudell, J.R. 2014, MNRAS, 442, 1239
 Press, W.H., Teukolsky, S.A., Vetterling, W.T., Flannery, B.P., 1992, Numerical Recipes. The Art of Scientific Computing, Cambridge University Press, Cambridge
 Shen, Y., Richards, G.T., Strauss, M.A. 2011, ApJS, 194, 45
 Shurtleff, R., 2013, arXiv:1311.6118
 Simmons, J. F. L., Stewart, B. G. 1985, A&A, 142, 100
 Smith, J.E., Robinson, A., Alexander, D.M., et al. 2004, MNRAS, 350, 140
 Sluse, D., Hutsemékers, D., Lamy, H., Cabanac, R., Quintana, H. 2005, A&A, 433, 757
 Tempel, E., Libeskind, N.I. 2013, ApJ, 775, L42
 Trowland, H.E., Lewis, G., Bland-Hawthorn, J. 2013, ApJ, 762, 72
 Wardle, J. F. C., Kronberg, P. P. 1974, ApJ, 194, 249
 Wills, B.J., Browne, I.W.A. 1986, ApJ, 302, 56
 Yadav, J.K., Bagla, J.S., Khandai, N. 2010, MNRAS, 405, 2009
 Zhang, Y., Yang, X., Wang, H., et al. 2013, ApJ, 779, 160

Table 1. The linear polarization of 93 quasars

Object	z	LQG	Date (dd/mm/yy)	q (%)	u (%)	p (%)	σ_p (%)	p_0 (%)	θ ($^\circ$)	σ_θ ($^\circ$)	Notes
SDSSJ104938.22+214829.3	1.2352	1	25/03/14	-0.02	0.00	0.02	0.07	0.00	–	–	
SDSSJ105140.40+203921.1	1.1742	1	22/03/14	-0.01	-0.14	0.14	0.06	0.13	133	13	
SDSSJ105224.08+204634.1	1.2032	1	23/03/14	-0.18	-0.02	0.18	0.10	0.16	93	18	
SDSSJ105258.16+201705.4	1.2526	1	23/03/14	-0.09	0.24	0.26	0.21	0.19	55	32	
SDSSJ105421.90+212131.2	1.2573	1	23/03/14	-1.04	-0.09	1.04	0.08	1.04	93	2	
SDSSJ105446.73+195710.5	1.2195	1	22/03/14	-1.64	0.93	1.89	0.23	1.88	75	4	
SDSSJ105525.18+191756.3	1.2005	1	23/03/14	-0.16	0.34	0.38	0.13	0.36	58	10	
SDSSJ105556.22+184718.4	1.2767	1	23/03/14	0.08	0.02	0.08	0.12	0.00	–	–	
SDSSJ105611.27+170827.5	1.3316	1	25/03/14	0.01	1.29	1.29	0.08	1.29	45	2	
SDSSJ105714.02+184753.3	1.2852	1	24/03/14	-0.02	-0.05	0.05	0.09	0.00	–	–	
SDSSJ105805.09+200341.0	1.2731	1	23/03/14	0.13	0.17	0.21	0.09	0.19	26	13	
SDSSJ105832.01+170456.0	1.2813	1	22/03/14	-0.35	-0.09	0.36	0.16	0.33	97	14	
SDSSJ105840.49+175415.5	1.2687	1	24/03/14	0.14	-0.24	0.28	0.11	0.26	150	12	
SDSSJ105928.57+164657.9	1.2993	1	24/03/14	0.02	0.24	0.24	0.15	0.20	43	21	
SDSSJ110016.88+193624.7	1.2399	1	22/03/14	0.88	-0.72	1.14	0.23	1.12	160	6	
SDSSJ110039.99+165710.3	1.2997	1	22/03/14	-0.06	0.16	0.17	0.12	0.14	56	25	
SDSSJ104139.15+143530.2	1.2164	2	22/03/14	-0.21	0.14	0.25	0.16	0.21	73	22	
SDSSJ104321.62+143600.2	1.2660	2	24/03/14	-0.19	-0.11	0.22	0.10	0.20	105	14	
SDSSJ104430.92+160245.0	1.2294	2	22/03/14	-0.08	0.04	0.09	0.07	0.07	76	30	
SDSSJ104445.03+151901.6	1.2336	2	23/03/14	1.13	-0.53	1.25	0.11	1.25	168	3	
SDSSJ104520.62+141724.2	1.2650	2	23/03/14	0.19	0.01	0.19	0.12	0.16	1	22	
SDSSJ104604.05+140241.2	1.2884	2	22/03/14	-0.17	0.50	0.53	0.15	0.51	54	8	
SDSSJ104616.31+164512.6	1.2815	2	24/03/14	-1.24	0.13	1.25	0.11	1.25	87	3	
SDSSJ104624.25+143009.1	1.3620	2	23/03/14	-0.04	-0.20	0.20	0.10	0.18	129	16	
SDSSJ104813.63+162849.1	1.2905	2	22/03/14	-0.04	0.16	0.17	0.12	0.14	53	25	
SDSSJ104859.74+125322.3	1.3597	2	25/03/14	-0.02	0.72	0.72	0.13	0.71	46	5	
SDSSJ104915.66+165217.4	1.3459	2	23/03/14	-0.14	-0.51	0.53	0.09	0.52	127	5	
SDSSJ104922.60+154336.1	1.2590	2	22/03/14	-0.26	0.03	0.26	0.15	0.22	87	19	
SDSSJ104924.30+154156.0	1.2965	2	25/03/14	-0.14	0.16	0.21	0.12	0.18	66	19	
SDSSJ104941.67+151824.6	1.3390	2	24/03/14	0.51	-1.21	1.31	0.13	1.30	146	3	
SDSSJ104947.77+162216.6	1.2966	2	22/03/14	0.13	-0.01	0.13	0.14	0.00	–	–	
SDSSJ104954.70+160042.3	1.3373	2	23/03/14	-0.21	-0.29	0.36	0.17	0.32	117	15	
SDSSJ105001.22+153354.0	1.2500	2	25/03/14	-0.03	-0.02	0.03	0.11	0.00	–	–	
SDSSJ105042.26+160056.0	1.2591	2	25/03/14	0.01	0.20	0.20	0.08	0.18	44	12	
SDSSJ105104.16+161900.9	1.2502	2	22/03/14	0.24	-0.01	0.24	0.10	0.22	179	13	
SDSSJ105117.00+131136.0	1.3346	2	23/03/14	-0.37	0.46	0.59	0.22	0.55	64	11	
SDSSJ105119.60+142611.4	1.3093	2	25/03/14	0.18	0.03	0.18	0.10	0.16	5	18	
SDSSJ105122.98+115852.3	1.3085	2	23/03/14	0.01	-0.02	0.02	0.10	0.00	–	–	
SDSSJ105125.72+124746.3	1.2810	2	25/03/14	0.08	-0.06	0.10	0.08	0.07	160	31	RadioS
SDSSJ105132.22+145615.1	1.3607	2	22/03/14	-0.40	0.15	0.43	0.10	0.42	80	7	
SDSSJ105144.88+125828.9	1.3153	2	25/03/14	0.21	0.13	0.25	0.07	0.24	15	8	RadioS
SDSSJ105210.02+165543.7	1.3369	2	24/03/14	-0.16	-0.23	0.28	0.09	0.27	117	10	
SDSSJ105222.13+123054.1	1.3162	2	24/03/14	-0.08	0.32	0.33	0.13	0.31	52	12	
SDSSJ105223.68+140525.6	1.2483	2	22/03/14	0.27	0.41	0.49	0.11	0.48	28	7	
SDSSJ105245.80+134057.4	1.3544	2	25/03/14	0.65	1.15	1.32	0.11	1.32	30	2	RadioS
SDSSJ105257.17+105933.5	1.2649	2	24/03/14	0.54	-0.15	0.56	0.11	0.55	172	6	
SDSSJ105412.67+145735.2	1.2277	2	24/03/14	-0.18	-0.32	0.37	0.10	0.36	121	8	RadioS
SDSSJ105435.64+101816.3	1.2600	2	24/03/14	-0.03	0.09	0.10	0.08	0.07	55	31	
SDSSJ105442.71+104320.6	1.3348	2	24/03/14	0.71	-0.18	0.73	0.11	0.72	173	4	
SDSSJ105523.03+130610.7	1.3570	2	25/03/14	0.03	0.00	0.03	0.10	0.00	–	–	
SDSSJ105525.68+113703.0	1.2893	2	24/03/14	-0.36	2.52	2.55	0.10	2.55	49	1	RadioS
SDSSJ105541.83+111754.2	1.3298	2	25/03/14	-0.45	0.01	0.45	0.11	0.44	89	7	
SDSSJ105621.90+143401.0	1.2333	2	23/03/14	-0.42	0.13	0.44	0.13	0.42	82	9	
SDSSJ105637.49+150047.5	1.3713	2	25/03/14	-0.37	0.46	0.59	0.16	0.57	65	8	
SDSSJ105637.98+100307.2	1.2730	2	23/03/14	-0.08	0.16	0.18	0.12	0.15	58	23	
SDSSJ105655.36+144946.2	1.2283	2	24/03/14	-0.14	-0.05	0.15	0.13	0.10	99	39	
SDSSJ105855.33+081350.7	1.2450	3	23/03/14	-0.01	0.29	0.29	0.09	0.28	46	9	
SDSSJ110006.02+092638.7	1.2485	3	22/03/14	0.17	0.14	0.22	0.09	0.20	19	13	
SDSSJ110148.66+082207.1	1.1940	3	24/03/14	0.10	-0.19	0.22	0.14	0.18	149	22	

Table 1. continued.

Object	z	LQG	Date (dd/mm/yy)	q (%)	u (%)	p (%)	σ_p (%)	p_0 (%)	θ ($^\circ$)	σ_θ ($^\circ$)	Notes
SDSSJ110217.19+083921.1	1.2355	3	23/03/14	0.35	-0.02	0.35	0.12	0.33	178	10	
SDSSJ110504.46+084535.3	1.2371	3	25/03/14	0.10	-0.10	0.14	0.10	0.11	157	26	
SDSSJ110621.40+084111.2	1.2346	3	22/03/14	0.09	0.10	0.14	0.15	0.00	–	–	
SDSSJ110736.60+090114.7	1.2266	3	22/03/14	-0.42	0.08	0.43	0.11	0.42	85	8	RadioS
SDSSJ110744.61+095526.9	1.2228	3	25/03/14	0.44	0.25	0.51	0.08	0.50	15	5	
SDSSJ111007.89+104810.3	1.2097	3	23/03/14	0.01	0.55	0.55	0.12	0.54	45	6	
SDSSJ111009.58+075206.8	1.2123	3	24/03/14	0.67	1.68	1.81	0.17	1.80	34	3	
SDSSJ111416.17+102327.5	1.2053	3	26/03/14	0.26	0.02	0.26	0.08	0.25	3	9	
SDSSJ111545.30+081459.8	1.1927	3	24/03/14	-0.30	0.16	0.34	0.14	0.31	76	13	
SDSSJ111802.11+103302.4	1.2151	3	23/03/14	1.01	-3.84	3.97	0.10	3.97	142	1	
SDSSJ111823.21+090504.9	1.1923	3	24/03/14	-0.10	-0.01	0.10	0.18	0.00	–	–	
SDSSJ112019.62+085905.1	1.2239	3	23/03/14	0.38	-0.15	0.41	0.13	0.39	170	10	
SDSSJ112059.27+101109.2	1.2103	3	24/03/14	0.44	0.29	0.53	0.22	0.49	17	13	
SDSSJ112109.76+075958.6	1.2369	3	25/03/14	-0.01	0.33	0.33	0.08	0.32	46	7	
SDSSJ104114.06+034312.0	1.2633	4	26/03/14	-0.26	0.41	0.49	0.16	0.46	61	10	BAL
SDSSJ104115.58+051345.0	1.2553	4	26/03/14	-0.14	0.27	0.30	0.13	0.27	59	14	
SDSSJ104116.79+035511.4	1.2444	4	26/03/14	-1.46	-0.51	1.55	0.11	1.55	100	2	LoBAL
SDSSJ104225.63+035539.1	1.2293	4	26/03/14	0.48	0.50	0.69	0.08	0.69	23	3	
SDSSJ104256.38+054937.4	1.3555	4	26/03/14	0.20	-0.36	0.41	0.12	0.39	149	9	
SDSSJ104425.80+060925.6	1.2523	4	26/03/14	-0.36	-0.20	0.41	0.11	0.40	105	8	BAL
SDSSJ104637.30+075318.7	1.3635	4	26/03/14	0.04	0.09	0.10	0.07	0.08	34	25	RadioS
SDSSJ104733.16+052454.9	1.3341	4	26/03/14	0.04	-0.19	0.19	0.07	0.18	142	11	
SDSSJ105010.05+043249.1	1.2158	4	26/03/14	-2.46	-1.04	2.67	0.08	2.67	102	1	RadioS
SDSSJ105018.10+052826.4	1.3067	4	26/03/14	-0.11	0.24	0.26	0.10	0.24	57	12	
SDSSJ105422.47+033719.3	1.2278	4	26/03/14	-0.18	-0.28	0.33	0.11	0.31	118	10	RadioS
SDSSJ105423.26+051909.8	1.2785	4	26/03/14	0.13	0.22	0.26	0.09	0.25	30	11	BAL
SDSSJ105512.23+061243.9	1.3018	4	26/03/14	-0.61	-0.77	0.98	0.12	0.97	116	4	
SDSSJ105534.66+033028.8	1.2495	4	26/03/14	-0.09	0.38	0.39	0.09	0.38	52	7	
SDSSJ105537.63+040520.0	1.2619	4	26/03/14	-0.10	0.02	0.10	0.11	0.00	–	–	
SDSSJ105719.23+045548.2	1.3355	4	26/03/14	-0.36	0.44	0.57	0.13	0.56	65	7	RadioS
SDSSJ105821.28+053448.9	1.2540	4	26/03/14	0.09	0.06	0.11	0.10	0.06	15	47	
SDSSJ105833.86+055440.2	1.3222	4	25/03/14	0.15	0.60	0.62	0.21	0.59	38	10	
SDSSJ110108.00+043849.6	1.2516	4	25/03/14	0.52	0.66	0.84	0.10	0.83	26	3	
SDSSJ110412.00+044058.2	1.2554	4	25/03/14	0.15	-0.08	0.17	0.11	0.14	167	22	

Notes. Column 1 gives the quasar SDSS name, column 2 the redshift z , column 3 the quasar group (1,2,3 = Huge-LQG, 4 = CCLQG; see also Fig. 4), column 4 the observation date, columns 5–6 the q and u normalized Stokes parameters corrected for the offset angle, column 7 the polarization degree p , column 8 the error on the polarization degree $\sigma_p \approx \sigma_q \approx \sigma_u$, column 9 the polarization degree p_0 debiased according to the Wardle and Kronberg (1974) method (see also Simmons and Stewart 1985), column 10 the polarization position angle θ , defined between 0° and 180° and measured in the equatorial coordinate system (North = 0° and East = 90°), and column 11 the error of the polarization angle estimated using $\sigma_\theta = 28.65^\circ \sigma_p/p_0$ to avoid underestimation at low signal-to-noise (Wardle and Kronberg 1974). Additional characteristics of the targets were retrieved from the NASA/IPAC Extragalactic Database (NED) and given in column 12: radio-source (RadioS), broad absorption line (BAL) quasar, and low-ionization BAL (LoBAL) quasar.